Chapter

Introductory Chapter: Advanced Ocean Current Simulation from TanDEM Satellite Data

Maged Marghany

1. Introduction

Satellite microwave data, such as synthetic aperture radar (SAR), have the great potential for retrieving ocean dynamic parameters, for instance, ocean surface current and ocean wave dynamic [1]. One of the attention-grabbing topics is current flow that is needed for short go back satellite cycle and high resolution. These will provide precisely data concerning current dynamic flow [2, 3]. In fact, current is very important for ship navigation, fishing, waste matter substances transport, and sediment transport [4, 5]. Respectively, optical and microwave sensors are enforced to monitor the current flows. Indeed, the ocean surface dynamic options of sea surface current are vital parameters for atmospheric-sea surface interactions. In this regard, the global climate change, marine pollution, and coastal risky are preponderantly dominated by current speed and direction [1]. The measurements of ocean current from space rely on the electromagnetic signal. Truly, associate degree of an electromagnetic signal of optical and microwave reflects from the ocean carrying records concerning one among the first discernible quantities that are the color, the beamy temperature, the roughness, and also the height of the ocean [2].

Recently, the high resolution of SAR sensors such as TerraSar-X, RADARSAT-2, ALOS PALSAR, and the foremost three of the Italian satellite of COSMO-SkyMed have been commenced. Once the four satellites in the COSMO-SkyMed constellation are developed, they are conceivable functioning with a tiny resume time of a little hours [4]. Nevertheless, the initial three of the COSMO-SkyMed, ALOS PALSAR, and RADARSAT-2, satellite data are the cross-track interferometry, which do not allow determining neither coastal water flow nor coastal water level changing. In this regard, the TerraSAR-X satellite data use an along-track interferometric proficiency which simply permits the quantity of sea surface speed. Additionally, phase alterations between the coregistered pixels of an image pair are consistent to Doppler frequency shifts of the signal backscattered and according to line-of-sight velocities of the scatterers. In this view, phase alterations include influences of surface flows and of the dynamic of wave movement. Consequently, the retrieving of tidal current flow can be accurately achieved by both of TerraSAR-X and TanDEM-X. These can be depleted to regulate precisely coastal water height fluctuations. The TerraSAR-X can regulate perfectly the digital surface model (DSM), where depiction of surface-containing topographies exceeds the terrain height, for example, plants and constructions through precision of 2 m.

Moreover, TanDEM-X involves dual high-resolution imaging SAR data. In this understanding, both TerraSAR-X and TanDEM-X are hovering in tandem and establishing an enormous radar interferometer with an anticipated competence of creating a comprehensive DSM through a perpendicular resolution of 2 m, exceeding

whatever obtainable currently from space [4]. Consistent with Romeiser et al. [6], with the usual helical revolution configuration, the dual satellites ensure an along-track gap between 0 at the northern and southern utmost locations of the orbit and approximately 550 m over the equator, restrictive of the district of convenient base-lines for intersatellite interferometry above the sea surface to restricted space crews far-off the north and south. In districts of elongated along-track baselines, the data characteristic undergoes since sequential decorrelation of the signal backscattered. Nonetheless, the TanDEM-X geometry constructions acquire adjusted from period to period to enhance the cross-track interferometry performing in coastal water height fluctuations and surface stream flow attentions [7].

On the word of Yoon et al. [8], the phase computation is a foremost encounter to regulate surplus precise height. This is because the calculated phase differences are assumed as a wrapped phase of the primary quantities of a scale $-\pi$ to π, hence the actuality vague contained by multiples of 2π [2, 9, 10]. This technique generates phase leaps between nearby pixels. Smooth function is depleted to resolve phase leap through adding or detracting multiples of 2π. Subsequently, Ferraiuolo et al. [2] have developed the multichannel MAP height estimator as a function of a Gaussian Markov random (GMRF) to unravel the doubts of height retrieving from InSAR procedure. They initiated that the multichannel MAP height estimator has accomplished the phase gaps and tweaked the height contour as compared to predictable phase unwrapping set of rules, i.e., path-following algorithms and minimum-norm algorithms.

The foremost demonstrable of this experiment is to investigate the coastal water level and velocity changes using along-track interferometric synthetic aperture radar (ATInSAR) technique multichannel MAP height estimator.

2. Algorithm

The algorithm is implemented in this study, which is based on the multichannel MAP height estimator. It is depleted to retain the information of the sea surface level alterations. This algorithm is implemented from the consideration of Baselice et al. [9]. Succeeding Baselice et al. [9], the signal of interferometric phase can be articulated by the next mathematical Eq. (1) [9],

$$\phi_{sn} = \left\langle \left(\frac{4\pi}{\lambda R_0 \sin\theta} \right) B_{\perp n} h_s + \alpha \right\rangle_{2\pi}, \text{n} = 1, 2, ..., \text{N}; s = 1, 2, ..., \text{S} \tag{1}$$

where s is the pixel locus in the TanDEM-X data, n is the deliberated interferogram band, λ is the TanDEM-X wavelength, R_0 is the stretch between the epicenter of the sight and the controlling antenna, and $B_{\perp n}$ is the orthogonal baseline. Furthermore, h_s is the height rate in meter, α is the phase decorrelation noise, and an incident angle is presented by θ. Moreover, $\langle . \rangle_{2\pi}$ signifies the "modulo-2π." Let us assume that N is autonomous interferogram bands; thenceforth, the obstruction contains the retrieving of the sea-level height rates h_s, which is being from the $S \times N$ as a function of the expected wrapped phase ϕ_{sn}. Succeeding Ferraiuolo et al. [2], the obstruction of demonstrating height can be elucidated by means of a MAP height approximation technique. In this understanding, the multichannel probability function F_{mc} is formulated as:

$$F_{mc}(\phi_s|\varsigma_s) = \prod_{n=1}^{N} f((\phi_{sn}|\varsigma_s) \tag{2}$$

here $F(\phi_{sn}|\varsigma_s)$ is the likelihood function of the signal channel, ϕ_s is calculated as wrapped phase data which is denoted as the pixel s, $\phi_s = [\phi_{s1}, \phi_{s2}, ..., \phi_{sN}]^T$, and ς_s

is collected vector height values where $\varsigma = [\varsigma_1, \varsigma_2, ..., \varsigma_S]^T$. Succeeding Baselice et al. [9] and Ferraiuolo et al. [2], a MAP algorithm height approximation can be casted by:

$$\widehat{\varsigma_{MAP}} = \arg_{\varsigma}\max\ln\left[\left(\prod_{S=1}^{S} F_{mc}(\phi_s|\varsigma_s)g(\varsigma;\hat{\sigma})\right]\right. \tag{3}$$

here $g(.)$ is a preceding probability density function (pdf) which is approved by means of Gaussian Markov random field (GMRF) and $\hat{\sigma}$ is the hyperparameter route which is not a preceding identified. As said by Baselice et al. [9], GMRF can be appraised beginning from the restrained interferograms. This is realized by deliberating subbands, equivalent to diverse azimuth looks. In this regard, GMRF is determined by:

$$g(\varsigma, \hat{\sigma}) = \frac{1}{Z(\sigma)} e^{\left(-\sum_{S=1}^{SxN}\sum_{K\in N_S}\left[\frac{(\varsigma_s-\varsigma_k)^2}{2\sigma_{sk}^2}\right]\right.} \tag{4}$$

where N_s is the district system of s^{th} pixel, and s is well known as hyperparameters, which are illustrative of the confined physical appearance of the sea-level height h, σ is the hyperparameter vector assembling all pixel values, and Z(σ) is the detachment function [10] which is required to standardize the pdf [2, 9, 10]. Lastly, the regularized restoration square error is estimated via:

$$\varepsilon = \frac{\|\hat{\varsigma} - \varsigma\|^2}{\|\varsigma\|^2} \tag{5}$$

where ς is the sea-level height which is derived from Eq. (3) and the accurate height then can be estimated from Eq. (4) ($\hat{\varsigma}$). Though the reform is deliberating the restricted sum of accessible data (four bands), it is virtuous to recover its feature, predominantly on the disjointedness. Formerly, inverse algorithm is executed to repossess the sea surface current pattern.

3. Dataset

Two panaches of acquaintance are required to inverse the sea surface current pattern which are: (i) TanDEM-X of SAR; and (ii) real in situ measurements throughout TanDEM-X satellite overpassed.

3.1 Satellite TanDEM-X data

Pair of Terra-SAR satellite data is attained by the TanDEM-X satellite on May 6, 2017. The earliest date was attained at 7:27:17 am; however, the subsequent data obtained at 19:20:06 pm. Both data are in spotlight mode with X-band and HH and VV polarization, respectively. Both spotlight modes are formatted in single look complex binary data. The TanDEM-X functioning concern encompasses the synchronized maneuver of two satellites hovering in contiguous pattern. The modification restraints for the construction are: (i) the revolution arising nodes, (ii) the perspective between the perigees, (iii) the revolution peculiarities, and (iv) the phasing between the satellites. The adherence of ocean surface flow is a vigorous façade of evaluating climate variations. Space-borne SAR along-track interferometry (ATI) obligates the talent to greatly subsidize to the contemporary field.
It will recommend a great-area, global-widespread seeming surface flow quantities.

The difficulties of representing comparatively low-slung speeds are regular resolute by the developments of SAR satellites that produce satisfactorily considerate ATI quantities [7].

In this revision, the multichannel MAP height estimator relies on the TanDEMX facts. Both TerraSAR-X and TanDEM-X satellites transmit identical SAR devices functioning at 9.65 GHz frequency (X-band). All over approximately dedicated maneuvers, both satellites are positioned acquaintance exceptionally in an actual singular track conformation through a fleeting along path reference line delivering a possibility for sea surface flow quantities. The TanDEM-X data exploited in this investigation were bistatic (TS-X active/TD-X passive) channel with VV polarization and in stripmap (SM) [6, 7].

3.2 In situ ocean current measurement

Succeeding Marghany [3], the device of Aquadopp® 2 MHz current meter was used to acquire the physical information of sea surface flows, for instance, speed and direction (**Figure 1**). In this view, the surface flow information achievement

Figure 1.
Deployment of Aquadop 2 MHz current meter in the coastal water.

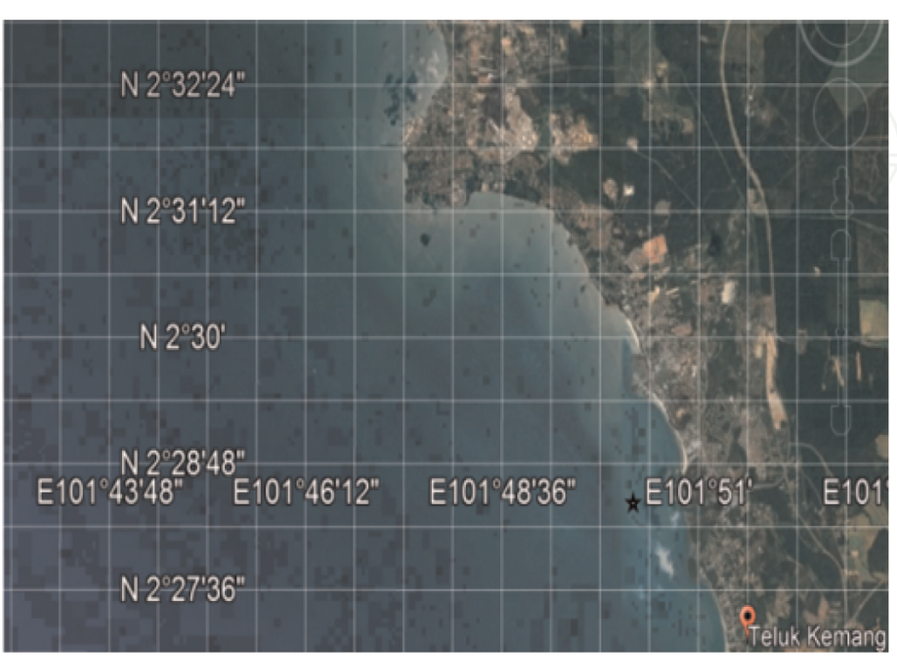

Figure 2.
In situ measurements geographical location.

was collected by the Aquadopp® 2 MHz current meter factory-made by Nortek AS, Scandinavian country. The device could be a standalone composition, manipulation of the Doppler-established frequency equipment to gauge the surface current flows at the positioning of a fixed geographical location on the sea surface. The equipment is envisioned basically with memory and internal battery pack somewhere it may be intended to tape and collect information within for self-positioning [3].

Along the coastal water of Teluk Kemang, Port Dickson, Malaysia, the current meter instrument of Aquadopp® 2 MHz current meter was arrayed on May 6, 2017 (**Figure 2**). Two periods of data collection were carried out: (i) at 6:15 am to 8:15 am and (ii) at 6:15 pm to 8:15 pm. For both phases, therefore, the surface flows were deliberated for intermissions of 2 h.

4. Current pattern from TanDEM-X data

The TanDEM-X satellite data with the spotlight of VV polarization are implemented to retrieve the sea surface flow rates (**Figure 3**). The retrieving sea level and sea surface flow variations are constrained to range direction. In fact, the sea surface current is only sensed along the range, while the wave spectra information is a function of SAR azimuth direction. The retrieving sea surface flows are delivered inshore zone of the coastal water of the Teluk Kemang, Port Dickson as part of the Malacca Straits.

Therefore, the Doppler shift frequency of the ATI indicates fluctuations of sea surface flow. The inshore water has a weak flow along 5 km of the coastal water. This is indicated by the lower rate value of 0.1 m/s. In this regard, the lowest spectral peak of the Doppler frequency shift is 0.04 which is corresponding to the frequency shift value of −200 Hz (**Figure 4**). In this view, the weak inshore water flow could be attributed to the impact of the low tide of 0.3 m as noticed along the coastal water of the Teluk Kemang, Port Dickson.

The interferogram phase is ranged between −0.7° and +0.7° (**Figure 5**) derived by the multichannel MAP height estimator. Obviously, the same pattern is visible.

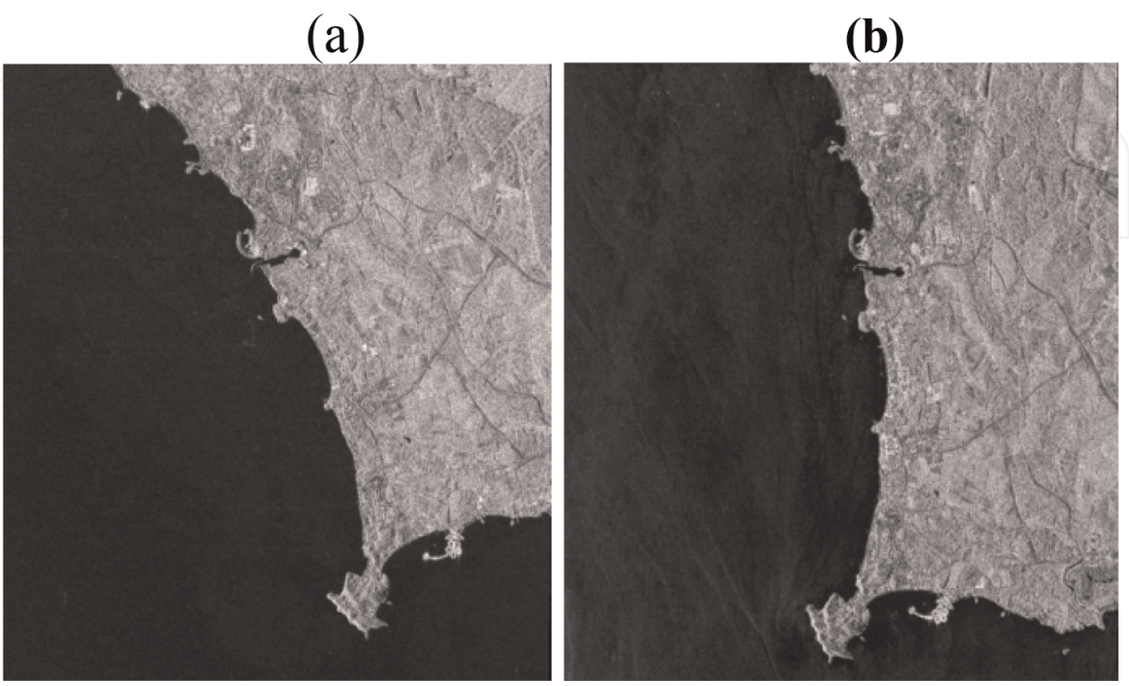

Figure 3.
TanDEM-X SAR data (a) first mission and (b) second mission with VV polarization.

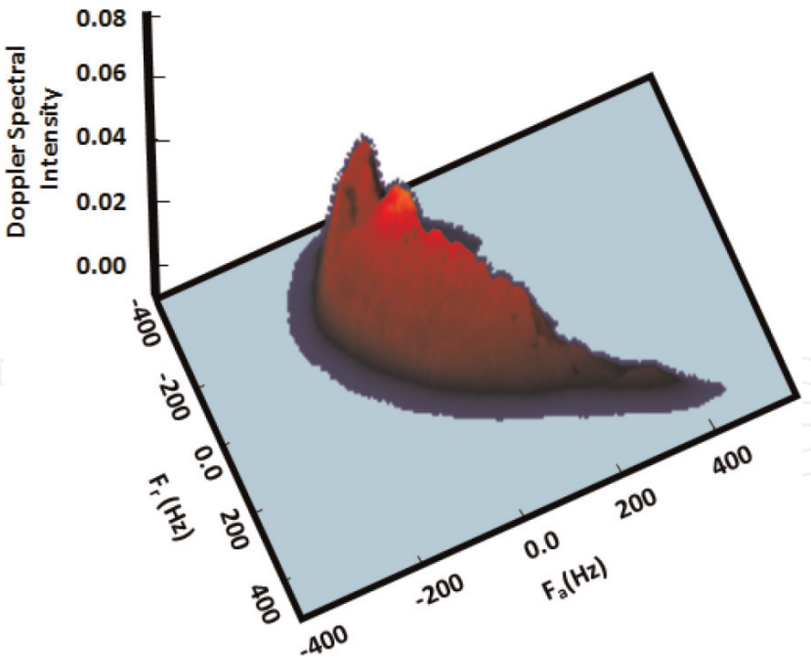

Figure 4.
TanDEM-X data Doppler spectra intensity.

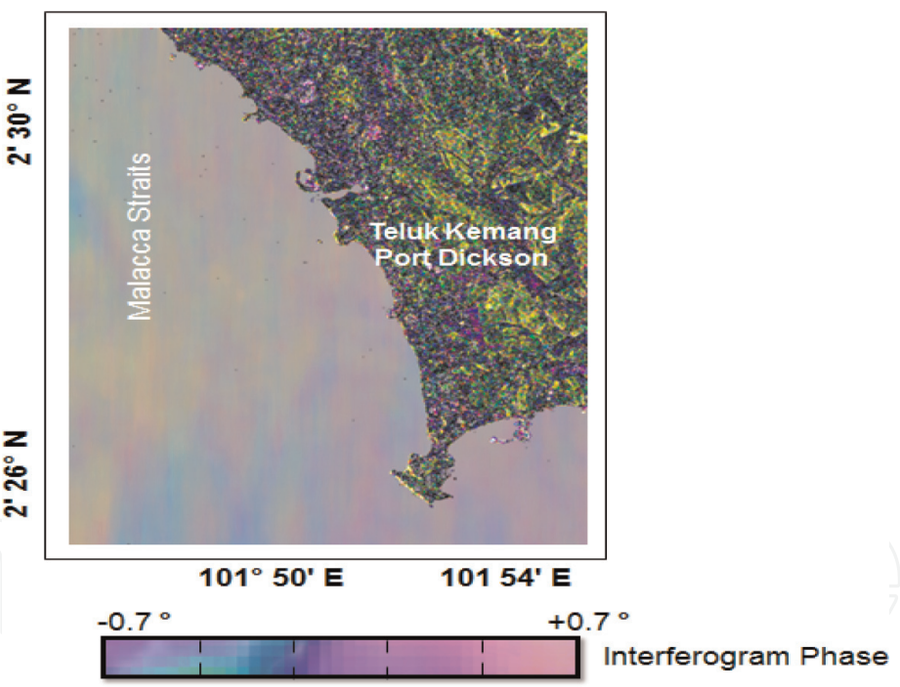

Figure 5.
Pattern of interferogram phase.

This pattern signature represents current feature variations along the coastal waters. Conversely, this interferogram phase is dominated by noises.

The inverters of the interferogram phase can be used to compute the ATI Doppler sea surface current. The ATI Doppler shows a clear current pattern movement along the coastal waters with minimum and maximum speed of 0.1 and 0.2 m/s, correspondingly (**Figure 6**). In fact, the interferometric combination of the two images reveals phase alterations that are comparable to the backscatter variations of the Doppler frequency shift [7]. This rapidity is conforming to sea-level differences of 0.4 m (**Figure 6**).

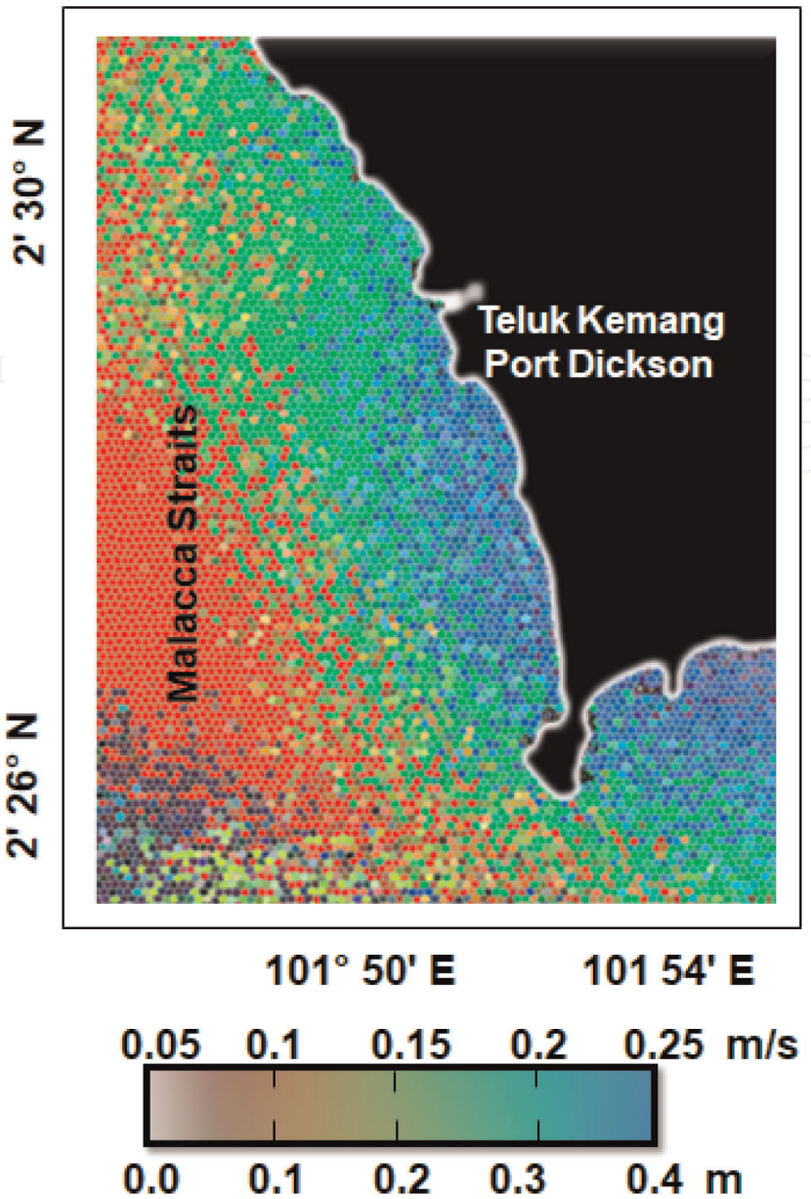

Figure 6.
Sea surface current and sea-level variations retrieved using an ATI MAP algorithm.

Figure 6 exhibits noteworthy correspondences between the consequence of sea surface flow speeds, which are created from TanDEM-X satellite data, and the consequence delivered in the in situ quantity. **Figure 7** demonstrates how the correlation coefficient alteration as direct correlation between the two different parameters is modified. Indeed, the investigation of the correlation between different measured parameters can assist to develop accurate model. Obviously, there is a worthy correlation between the retrieved sea surface flow and real in situ measured flow with r^2 of 0.76. Conversely, this correlation is not faultless, but it appears to have a confident, direct association, and resembles to what one would guess when bearing in mind both sea surface flow simulation from satellite data and one is measured in situ and then follow the hypothesis of normality.

As said by Romeiser et al. [6, 7], the signatures of the Doppler frequency shift are clearly responsive to sea surface flow than to wind modifications. Similarly, a modification of the Doppler frequency shifts has a tiny effect on the TanDEM-X backscatter intensity as compared to relaxation rate. Obtaining phase by using multichannel MAP height estimator algorithm will allow us to characterize the water sea-level fluctuations. Three-dimensional reconstruction of water-level

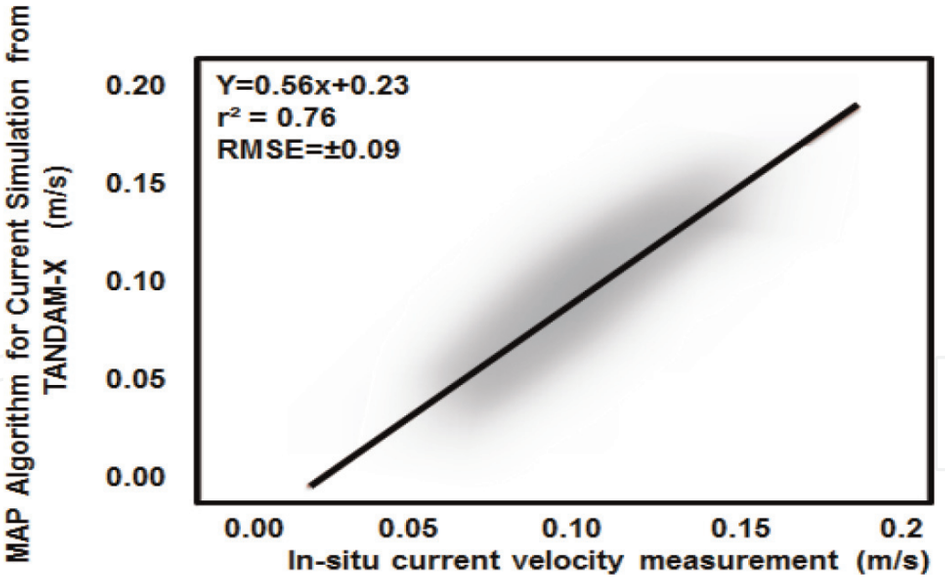

Figure 7.
Validation of MAP algorithm with in situ measurement.

changes from the ATInSAR technique by using the algorithm of multichannel MAP height approximation can aid to regulate the vertical shift of sea-level changes. Moreover, the multichannel MAP height approximation has achieved the difficulty of the phase unwrapping discontinuities and amended the vertical displacement synopsis as rivaled to conservative algorithm of phase unwrapping, for instance, (i) minimum-norm algorithm and (ii) path-following algorithm [9]. Lastly, TanDEM-X satellite data are comprehended as the prospective radar device for observing the dynamic fluctuation of ocean surface. Sea surface flow is considered as one of a consideration—impressing issue which is required a short visit cycle and extraordinary resolution. In this understanding, these can afford specific facts in relation to sea surface dynamic flow [2, 3, 5, 9–16].

5. Conclusion

This work has revealed a method for regaining sea surface flow using such high-resolution satellite data of TanDEM SAR-X. Along-track interferometry (ATI) technique is implemented to retrieve sea surface current movement. To this end, multichannel MAP height estimator algorithm is said to model sea-level variation. Then, the inverse algorithm is used which is based on the Doppler frequency model to retrieve sea surface current. The results reveal that the sea surface flow pattern is dominated by low velocity of less than 0.3 m/s which corresponds to lower sea-level variation of 0.4 m. The study confirms that multichannel MAP height estimator algorithm is proficient to regain the sea surface flow rate from ATI TanDEM-X with an extraordinary precision of ±0.09 m/s. In conclusion, the approximation algorithm of multichannel MAP height conceivably can be a tremendous practice for repossessing sea surface flow pattern and sea-level fluctuations from ATI TanDEM-X satellite data.

DOI: http://dx.doi.org/10.5772/intechopen.84644

Author details

Maged Marghany
Faculty Geospatial and Real Estate, Geomatika University College, Kuala Lumpur, Malaysia

*Address all correspondence to: magedupm@hotmail.com

References

[1] Lu Z, Kim J-W, Lee H, Shum C, Duan J, Ibaraki M, et al. Helmand river hydrologic studies using ALOS PALSAR InSAR and ENVISAT altimetry. Marine Geodesy. 2009;**32**(3):320-333

[2] Ferraiuolo G, Meglio F, Pascazio V, Schirinzi G. DEM reconstruction accuracy in multichannel SAR interferometry. IEEE Transactions on Geoscience and Remote Sensing. 2009; **47**(1):191-201

[3] Marghany M. Developing robust model for retrieving sea surface current from RADARSAT-1 SAR satellite data. International Journal of Physical Sciences. 2011;**6**(29):6630-6637

[4] Mason DC, Speck R, Devereux B, Schumann GJ-P, Neal JC, Bates PD. Flood detection in urban areas using TerraSAR-X. IEEE Transactions on Geoscience and Remote Sensing. 2010; **48**(2):882-894

[5] Marghany M. Three-dimensional visualisation of coastal geomorphology using fuzzy B-spline of dinsar technique. International Journal of Physical Sciences. 2011;**6**(30):6967-6971

[6] Romeiser R, Runge H. Theoretical evaluation of several possible along-track InSAR modes of TerraSAR-X for ocean current measurements. IEEE Transactions on Geoscience and Remote Sensing. 2007;**45**(1):21-35

[7] Romeiser R, Runge H, Suchandt S, Kahle R, Rossi C, Bell PS. Quality assessment of surface current fields from TerraSAR-X and TanDEM-X along-track interferometry and Doppler centroid analysis. IEEE Transactions on Geoscience and Remote Sensing. 2014; **52**(5):2759-2772

[8] Yoon G-W, Kim S-W, Lee Y-W, Won J-S. Measurement of the water level in reservoirs from TerraSAR-X SAR interferometry and amplitude images. Remote Sensing Letters. 2013; **4**(5):446-454

[9] Baselice F, Ferraioli G, Pascazio V. DEM reconstruction in layover areas from SAR and auxiliary input data. IEEE Geoscience and Remote Sensing Letters. 2009;**6**(2):253-257

[10] Ferraiuolo G, Pascazio V, Schirinzi G. Maximum a posteriori estimation of height profiles in InSAR imaging. IEEE Geoscience and Remote Sensing Letters. 2004;**1**(2):66-70

[11] Marghany M. Three-dimensional coastal geomorphology deformation modelling using differential synthetic aperture interferometry. Zeitschrift fur Naturforschung A: Journal of Physical Sciences. 2012;**67**(6):419

[12] Marghany M. DEM reconstruction of coastal geomorphology from DINSAR. In: Murgante B et al., editors. Lecture Notes in Computer Science (ICCSA 2012). Part III, LNCS 7335. New York City: Springer; 2012. pp. 435-446

[13] Marghany M. DInSAR technique for three-dimensional coastal spit simulation from radarsat-1 fine mode data. Acta Geophysica. 2013;**61**(2):478-493

[14] Marghany M. Simulation of Tsunami Impact on Sea Surface Salinity along Banda Aceh Coastal Waters, Indonesia. In: Marghany M, editors. Advanced Geoscience Remote Sensing. Croatia: Intech; 2014. pp. 229-251

[15] Marghany M. Hybrid genetic algorithm of interferometric synthetic aperture radar for three-dimensional coastal deformation. In: Hybrid Genetic Algorithm of Interferometric Synthetic Aperture Radar for Three-Dimensional Coastal Deformation. 2014. pp. 116-131

[16] Marghany M. Simulation sea surface current from RADARSAT-2 SAR data using Hopfield neural network. In: Synthetic Aperture Radar (APSAR), 2015 IEEE 5th Asia-Pacific Conference on Synthetic Aperture Radar (APSAR). New York: Institute of Electrical and Electronics Engineers (IEEE); 2015. pp. 805-808